



## RESEARCH REPOSITORY

*This is the author's final version of the work, as accepted for publication following peer review but without the publisher's layout or pagination.  
The definitive version is available at:*

<https://doi.org/10.1016/j.jmbbm.2017.05.018>

**Miramini, S., Smith, D.W., Zhang, L. and Gardiner, B.S. (2017) The spatio-temporal mechanical environment of healthy and injured human cartilage during sustained activity and its role in cartilage damage. *Journal of the Mechanical Behavior of Biomedical Materials*, 74 . pp. 1-10.**

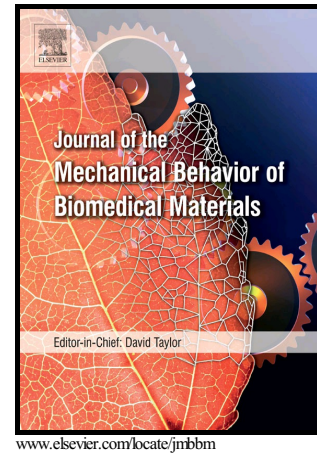
<http://researchrepository.murdoch.edu.au/id/eprint/36761>

Copyright: © 2017 Elsevier Ltd  
It is posted here for your personal use. No further distribution is permitted.

## Author's Accepted Manuscript

The spatio-temporal mechanical environment of healthy and injured human cartilage during sustained activity and its role in cartilage damage

Saeed Miramini, David W. Smith, Lihai Zhang, Bruce S. Gardiner



PII: S1751-6161(17)30206-0  
DOI: <http://dx.doi.org/10.1016/j.jmbbm.2017.05.018>  
Reference: JMBBM2335

To appear in: *Journal of the Mechanical Behavior of Biomedical Materials*

Received date: 19 January 2017  
Revised date: 5 May 2017  
Accepted date: 9 May 2017

Cite this article as: Saeed Miramini, David W. Smith, Lihai Zhang and Bruce S Gardiner, The spatio-temporal mechanical environment of healthy and injured human cartilage during sustained activity and its role in cartilage damage *Journal of the Mechanical Behavior of Biomedical Materials* <http://dx.doi.org/10.1016/j.jmbbm.2017.05.018>

This is a PDF file of an unedited manuscript that has been accepted for publication. As a service to our customers we are providing this early version of the manuscript. The manuscript will undergo copyediting, typesetting, and review of the resulting galley proof before it is published in its final citable form. Please note that during the production process errors may be discovered which could affect the content, and all legal disclaimers that apply to the journal pertain

## The spatio-temporal mechanical environment of healthy and injured human cartilage during sustained activity and its role in cartilage damage

Saeed Miramini<sup>a\*</sup>, David W. Smith<sup>b1</sup>, Lihai Zhang<sup>c2</sup>, Bruce S. Gardiner<sup>d3</sup>

<sup>a</sup>Department of Infrastructure Engineering, The University of Melbourne, Victoria 3010, Australia

<sup>b</sup>Faculty of Engineering, Computing and Mathematics, The University of Western Australia, WA, 6009, Australia

<sup>c</sup>Department of Infrastructure Engineering, The University of Melbourne, VIC 3010, Australia

<sup>d</sup>School of Engineering and Information Technology, Murdoch University, WA, 6150, Australia

s.miramini@unimelb.edu.au

david.smith@uwa.edu.au

lihzhang@unimelb.edu.au

b.gardiner@murdoch.edu.au

\*Corresponding author. Tel: +(613) 83449696; Fax: +(613) 83444616.

### Abstract

Recently we presented a computational model of articular cartilage calibrated for normal human tissue explants. This model was able to capture the transient deformation of cartilage experiencing a cyclic load. The model takes into account the tension-compression nonlinearity of the cartilage and incorporates the dependency of the compressive stiffness and fluid permeability of cartilage on the deformation-dependent aggrecan concentration in cartilage tissue. As such it represents a leading constitutive model of articular cartilage. Here we build on the previous study to develop an experimentally validated computational

---

<sup>1</sup> Tel: +(618) 6488 5531; Fax: +(618) 6488 1089

<sup>2</sup> Tel: +(613) 83447179; Fax: +(613) 83444616

<sup>3</sup> Tel: +(618) 93606505T

model to simulate mechanical consolidation response of intact and previously injured cartilage under sustained static loading, to develop our understanding of the implications for rates of tissue damage. We see that the type of prior injuries compromise the cartilage function in different ways. Relatively rapid consolidation is predicted for cartilage with a complete meniscectomy and that with a full thickness defect, indicating the inability of cartilage with such injuries to sustain interstitial fluid pressurisation for long periods of time, as does uninjured cartilage. By comparing the consolidation response of articular cartilage predicted by computational model against experimental measurements of the apparent friction coefficient following static loading, we find a strong linear positive correlation exists between cartilage degree of consolidation (DoC) and friction coefficient at the joint. As the DoC of articular cartilages can be estimated *in vivo* via medical imaging, the DoC can be used as an index to non-invasively evaluate the apparent friction coefficient between opposing cartilage surfaces, and so estimate the likelihood of frictional surface wear and/or cartilage damage.

**Keywords:**

Articular cartilage; Meniscectomy; Cartilage defect; Friction coefficient; Medical imaging; Knee health assessment

**1. Introduction**

Articular cartilage is a multiphasic material. However it is often treated mathematically using two phases: a solid phase comprising collagen, proteoglycans, other proteins, and chondrocytes and fluid phase comprising water and electrolytes (Gardiner et al., 2007; Kwan et al., 1984; Mow and Huiskes, 2005; Pierce et al., 2013; Soltz and Ateshian, 2000; Zhang et al., 2007). When cartilage is subjected to compressive loading, the load is initially carried by the fluid phase. As interstitial fluid exudes through the tissue surface, load

is transferred to the solid matrix. Time dependent fluid drainage leads to a time dependent deformation of the cartilage tissue known as consolidation (Verruijt, 2013).

As a material with multiple biological functions, articular cartilage faces several difficult biomechanical challenges. It experiences high loads, stresses and deformations during normal use. The human knee cartilage experiences contact forces up to 5 times of body weight during stair climbing (Taylor et al., 2004). Yet at the same time as experiencing high contact stresses, it achieves very low friction. Cartilage on cartilage friction coefficients are in the range 0.005-0.02 (Longmore and Gardner, 1975; Merkher et al., 2006). This friction coefficient is lower than all manufactured 'slippery' surfaces (McNary et al., 2012; Mow et al., 1992). Low friction is important, as friction is the principal cause of wear at contacting surfaces. But it is important to recognise that the (apparent) friction coefficient increases with time, and so a long period of static loading with attendant consolidation of the cartilage followed by movement, can result in much larger friction coefficients (Forster and Fisher, 1996). The consolidation deformations associated with the larger apparent friction coefficients may lead to greatly increased surface wear and cartilage tissue damage. This implies that the details of the time-dependent load patterns are a crucially important consideration when attempting to assess the likely impact of activities on joint health (Gardiner et al., 2016).

In this study, we hypothesize that the duration of cartilage loading relative to the characteristic time for cartilage consolidation plays an important role in determining the friction coefficient (and so the rate of cartilage damage and wear). For example, a long duration of continuous usage may significantly compromise cartilage's famously low friction coefficient, thereby exposing it to increased shear stresses and rates of wear, while larger volumetric and shear deformations increase the rate of extracellular matrix damage which

may potentially lead to cell death. A corollary of this hypothesis is that the degree of consolidation (DoC) of the cartilage should also be related to the apparent friction coefficient. We speculate that the DoC is strongly correlated with damage potential of cartilage tissue. This is potentially of great practical interest not only conceptually, but because the DoC can be estimated via *in vivo* imaging based on the time dependent closure of the joint space. In contrast, excess interstitial fluid pressure, exudate fluid volume and effective contact stresses cannot be practically measured *in vivo*.

The objective of this paper is to compare the mechanical consolidation response of articular cartilage to sustained periods of static loading, contrasting the consolidation response for intact and compromised cartilage or joint tissue to investigate the relationship between characteristic time for cartilage consolidation and friction coefficient. Specifically we will numerically study human tibial cartilage (lateral tibial plateau) for 5 different cases: (1) intact cartilage; (2) cartilage with partial meniscectomy; (3) cartilage with complete meniscectomy; (4) cartilage with a partial thickness defect; and (5) cartilage with a full thickness defect. In addition, we will investigate the possible correlation between DoC and apparent friction coefficient of articular cartilages.

## **2. Materials and Methods**

We have recently published a non-linear poroelastic model of human knee articular cartilage under cyclic loading (Zhang et al., 2015) and validated it against *in vitro* lab testing of osteochondral explants (Barker and Seedhom, 2001). We further develop our model to investigate the mechanical consolidation of cartilage for the 5 prototypical cases. We briefly summarise the model below.

### **2.1. Poroelastic cartilage model**

The cartilage extracellular matrix is treated as a fully saturated porous media, composed of interstitial fluid and solid phase. The total stress tensor  $\boldsymbol{\sigma}$  inside the cartilage tissue is the sum of solid and fluid Cauchy stress tensors as follows:

$$\boldsymbol{\sigma} = \boldsymbol{\sigma}^s + \boldsymbol{\sigma}^f = \boldsymbol{\sigma}_E^s - p\mathbf{I} \quad (1)$$

where  $p$  is the excess interstitial fluid pressure generated by loading the tissue,  $\mathbf{I}$  is the identity matrix and  $\boldsymbol{\sigma}_E^s$  is the incremental effective stress associated with the deformation of the solid phase. It should be noted that the analysis is an incremental analysis from the initial state. Excess interstitial fluid pressure, is the current interstitial fluid pressure minus the initial interstitial fluid pressure. The initial interstitial fluid pressure is assumed to be zero by definition. However, this ignores very small contributions to pressure that are in fact present e.g. gravitational.

Under the absence of body and inertial forces, the momentum equation can be expressed as:

$$\nabla \cdot \boldsymbol{\sigma} = 0. \quad (2)$$

The cartilage solid matrix can be modelled as an elastic solid with different properties in tension and compression (Soltz and Ateshian, 2000). This behaviour is due to the fact that collagen network governs cartilage's tensile properties while it does not support compression, whereas the aggrecan dominates the cartilage behaviour under slow or static compressive loads. Experimental studies have shown that a quadratic relationship exists between compressive stiffness of cartilage solid matrix and its aggrecan volume fraction (Treppo et al., 2000):

$$H_{-A} = a_1 \phi_G + a_2 \phi_G^2 \quad (3)$$

where  $H_{-A}$  is cartilage aggregate (osmotic) modulus (MPa),  $\phi_G$  (1) is the 'actual' aggrecan volume fraction of cartilage tissue and  $a_1$  (MPa) and  $a_2$  (MPa) are empirical constants. The cartilage aggregate modulus can be used to find the compressive elastic modulus of cartilage based on the following relation:

$$E_c = 3H_{-A}(1 - 2\nu) \quad (4)$$

where  $\nu$  is aggrecan effective Poisson's ratio (i.e. Poisson's ratio of aggrecan matrix without excess interstitial fluid pressure) which is usually found to be small, and is taken zero in this study (Schinagl, Ting et al. 1996).

It should be noted that, generally, the laboratory measurements of aggrecan volume fraction is an 'apparent' volume fraction defined as aggrecan volume over total cartilage volume. The 'apparent' volume fraction of aggrecan varies along the cartilage depth (see Table 1). However because a significant portion of the volume of articular cartilage is occupied by collagen fibrils and aggrecan can reside only within the extra-fibular domain, the aggrecan actually exists within cartilage at a higher local concentration or 'actual' volume fraction. In other words, the collagen volume fraction influences the 'actual' aggrecan volume fraction of cartilage and subsequently compressive stiffness. For example, if the collagen volume fraction (collagen volume over total cartilage volume) and the 'apparent' aggrecan volume fraction in the cartilage superficial region is  $\alpha=50\%$  and 60 mg/ml respectively, the 'actual' aggrecan volume fraction would be  $60/\alpha=120$  mg/ml.

In addition the aggrecan volume fraction varies due to cartilage volumetric deformation, based on the following mathematical equation:

$$\phi_G(t) = \frac{\phi_{G0}}{J^s(t) - \alpha} \quad (5)$$

where  $\phi_G(t)$  is 'actual' aggrecan volume fraction at time  $t$ ,  $\phi_{G0}$  is initial 'apparent' aggrecan volume fraction,  $J^s(t)$  is cartilage solid phase volume ratio (i.e. Jacobian determinant of the deformation gradient of solid phase  $=\det(\mathbf{F})$ ) and  $\alpha$  is collagen volume fraction of cartilage.

The cartilage collagen network is responsible for tensile stiffness of the cartilage matrix. The stiffness of collagen network in tension in a healthy cartilage is relatively high compared to aggrecan in compression. The tensile stiffness of cartilage matrix also varies with depth and orientation, corresponding to variation in the collagen volume fraction and fibre orientation. Table 2 shows the depth and orientation dependent tensile modulus of cartilage matrix applied in this study.

The continuity equation for the cartilage porous medium can be written as:

$$\nabla \cdot (\mathbf{v}_d + \mathbf{v}^s) = 0 \quad (6)$$

where  $\mathbf{v}_d = -k\nabla p$  is Darcy's velocity which has a linear relationship with the fluid pressure gradient  $\nabla p$ . The hydraulic permeability of cartilage tissue  $k$  ( $\text{m}^4/\text{N}\cdot\text{s}$ ) is negatively correlated with cartilage aggrecan volume fraction (Zamparo and Comper, 1989) and consequently influenced by cartilage deformation and can be expressed as:

$$k = \frac{n(\phi_G)^m}{\mu} \quad (7)$$

where  $\mu$  is interstitial fluid viscosity at 37 °C,  $n$  ( $\text{m}^2$ ) and  $m$  (1) are empirical parameters. It should be noted that we assume the aggrecan concentration leads to an isotropic permeability in the model, as aggrecan completely dominates the permeability of

cartilage. Table 1 and 2 shows the material properties and parameters applied in the model in this paper which are typical values for human knee cartilage.

## 2.2. *Model geometry and boundary conditions*

Figure 1 shows the model geometry and dimensions of a intact human lateral tibial plateau (Case 1) reconstructed based on MRI of lateral tibial plateau of a 35-year-old woman (Goodwin et al., 2004). We adopt an axisymmetric geometry and loading condition for lateral tibial plateau due to a reasonable assumption that lateral tibia plateau is remarkably symmetric within  $\pm 40^\circ$  of the mid-frontal plane (Hayes et al., 1978) and that the applied loading on lateral and medial tibia plateau is axisymmetric based on the reasonably axisymmetric contours of contact deformation observed in experiments (Marzo and Gurske-DePerio, 2009). It should be noted that, although a meniscus tear can alter the axisymmetric distribution of the load, as can be seen in the experimental observations of Marzo and Gurske-DePerio (2009), their experimental results show that the axisymmetric loading is restored following surgical repair (i.e. meniscectomy). As illustrated in Table 3, a wide range of tibio-femoral contact area has been reported in the literature, with a total contact area (lateral and medial plateau) of  $2000 \text{ mm}^2$  (Macquet Paul et al., 1975),  $1200 \text{ mm}^2$  (Marzo and Gurske-DePerio, 2009), to as low as  $520 \text{ mm}^2$  (Van de Velde et al., 2009). For the purpose of illustration, in this study we select an intermediate contact area from this range. Under physiologically-relevant loading condition, and in the presence of intact menisci, we assume the contact area of the medial and lateral tibial plateaus to be approximately equal, with the total contact area of  $1000 \text{ mm}^2$  for a healthy cartilage, which is reasonably consistent with that reported by Marzo and Gurske-DePerio (2009) and Fukubayashi and Kurosawa (1980). It is known that meniscectomy decreases tibio-femoral contact area and accordingly result in an increase in contact pressure. It was reported that the lateral plateau

contact area without the menisci (complete meniscectomy) is around 230 mm<sup>2</sup> (Fukubayashi and Kurosawa, 1980).

In this paper, we assume a compressive static load equivalent to 2.59 standard bodyweight (i.e. 2.59×750 N) is applied on the knee, representing the loading applied on one knee joint during one legged stance (Kutzner et al., 2010). We assume the load to be equally distributed between lateral and medial compartments of the knee. Therefore, we consider the lateral tibio-femoral contact area for the intact cartilage model (Case1, Figure 1) to be 500 mm<sup>2</sup> under a resultant force of  $F_R=970$  N representing the average contact condition for 'intact cartilage'. But the contact loading is not uniform and can be approximated by a parabolically-distributed compressive loading based on the contours of contact deformation observed in experiments (Marzo and Gurske-DePerio, 2009). For simplicity, in the current model we apply a conically-distributed loading on the cartilage, which appears to be a reasonable approximation to the contact pressure contours reported by Marzo and Gurske-DePerio (2009). A fixed, rigid and impervious subchondral bone substrate is employed for the model. In addition, a free flux condition was considered for the unloaded cartilage surface while a zero flux boundary condition was applied on cartilage surface beneath the loading (Ateshian et al., 1994) (Ateshian et al., 1994). The above describes the base case (Case 1) of an intact cartilage tissue.

We investigate the influence of partial (Case 2) and complete (Case 3) meniscectomy on mechanical behaviour of tibial cartilage by applying the same magnitude of compressive loading ( $F_R=970$  N) as for intact cartilage, but over a smaller contact area. We use contact area of 365 mm<sup>2</sup> and 235 mm<sup>2</sup> respectively for partial and complete meniscectomy (Fukubayashi and Kurosawa, 1980) (Figure 2). The reduced contact area for the

'meniscectomy models' relative to intact cartilage model, results in a higher peak loading per unit area as indicated in Figure 2 and Table 4. It should be noted that we assume the loading does not shift significantly within the meniscectomized joint compared to a normal joint as the menisci mainly widen the tibio-femoral contact area. This can be seen from the Fukubayashi and Kurosawa's experimental measurements of pressure distribution pattern for normal and meniscectomized knees (Fukubayashi and Kurosawa, 1980).

We also investigate the mechanical behaviour of cartilage with both a partial thickness (Case 4) and full thickness (Case 5) defect by applying the same magnitude of resultant force as applied on the intact cartilage model, but over a smaller surface of cartilage and with an annular conical loading distribution as shown in Figure 3. This leads to a larger load per unit area for cartilage with a defect in comparison to intact cartilage as illustrated in Figure 3.a and b. Importantly we consider a free flux boundary condition at the defect site as a result of the damage to the surrounding cartilage tissue. In other words, excess interstitial fluid pressure cannot be sustained at the defect site.

### 2.3. *Numerical solver settings*

We employ the poroelastic module of COMSOL Multiphysics to numerically solve the cartilage models in this study. The two-dimensional axisymmetric cartilage model is meshed with 5678 triangular elements with quadratic interpolation function. The time-dependent implicit solver of COMSOL Multiphysics with a relative tolerance of  $10^{-3}$  is applied to solve the finite element discretization of the time-dependent partial differential equations of the model under the described boundary conditions. Table 1 and 2 shows the material properties and parameters applied in the models which are typical values for human knee cartilage. The loading is ramped over 0.5 s to facilitate the numerical convergence of the

model and then kept constant for 14000 s (3.9 hr) to ensure complete consolidation in all cartilage models.

### 3. Results

Modelling results will be presented according to the key mechanical characteristics expected to have implications to cartilage wear and damage, namely: peak contact strain, consolidation rate, excess interstitial fluid pressure and fluid exudation rate.

#### 3.1. Contact strain

##### 3.1.1. Model validation

Figure 4a compares the time-evolution of peak contact strain for the five different cases. We define the peak contact strain as the maximum vertical deformation divided by cartilage thickness. It can be seen in Figure 4a that the intact cartilage (Case 1) is predicted to experience approximately 10% peak contact strain when the load is applied for 5 s. This prediction is consistent with the experimental results of Hosseini et al. (2010), who reported peak contact strain of  $8.6 \pm 2.6$  % in the lateral tibia plateau 5 s after application of full body weight to one leg. The model predicts a peak contact strain of 13.8%, 300 s after loading application which is also similar to the experimental measurements of Hosseini et al. (2010) (i.e.  $14.6 \pm 3.9$  % peak contact strain at  $t=300$  s). The model predicts a steady state peak contact strain of 25% for the intact cartilage which is also consistent with experimental measurements of Barker and Seedhom (2001) .

The largest peak contact strain is predicted for cartilage with a complete meniscectomy (Case 3). This prediction is due to the largest load per unit area being applied on the cartilage surface for the model with a complete meniscectomy (see Table 4). The

presence of an intact meniscus in the knee spreads the contact area and so distributes the load over a larger cartilage surface. This load spreading is impaired for a cartilage with partial and complete meniscectomy (McDermott and Amis, 2006).

Among the five models, the largest (maximum) load per unit area occurs with complete meniscectomy (Case 3), and this resulted in the largest contact pressure and the largest steady state peak contact strain of 35%. The model prediction shows a 40% increase in steady state peak contact strain for the cartilage with complete meniscectomy compared to that of the intact cartilage. This result is also in a good agreement with the experimental result of Song et al. (2008) that shows around 35% increase in steady state maximum strain of meniscectomized knees compared to that of intact knees.

### 3.2. Consolidation rate

The time taken to reach the maximum strain (time to steady state strain) is important, as it will determine how soon the tissue and cells are experiencing high strains following the onset of loading and/or physical activity. To study time dependent cartilage deformation, we plot the degree of consolidation (DoC) for each of the 5 Cases in Figure 4b. The DoC at time  $t$  is defined as:

$$DoC(t) = \frac{w(t) - w(0)}{w(t_{steady\ state}) - w(0)} \quad (8)$$

where  $w(t)$  is the peak contact deformation (with direction normal to the cartilage surface,  $z$ ) at time  $t$ ,  $w(0)$  is the initial peak contact deformation (i.e. deformation immediately after load application) and  $w(t_{steady\ state})$  is the steady state peak contact deformation. The DoC

varies between zero and one. The  $DoC \rightarrow 1$ , when the cartilage approaches its final deformed state under sustained load, and occurs when excess interstitial fluid pressure  $\rightarrow 0$ . Conversely, a small DoC indicates large excess interstitial fluid pressures and small tissue volumetric strain.

It can be seen that the intact cartilage model (Case 1) experiences the smallest DoC, among all the other models, at any given time prior to reaching steady state. This result suggests that the intact cartilage can support joint loading through interstitial fluid pressurization for a comparatively longer period of time.

The computational model prediction suggests that the cartilage with complete meniscectomy (Case 3) and that with a full thickness defect (Case 5) reach their maximum contact strain (full consolidation) earlier than all the other cases, in about 30minutes (see Table 4). This is due to the fact that, the excess interstitial fluid pressures gradients is largest for the cartilage with a complete meniscectomy as a result of both shorter drainage pathways and larger excess interstitial fluid pressures. On the other hand, the fluid exudate rate is highest for cartilage with full thickness defect as the drainage surface area is increased by the defect, resulting in a quick consolidation. The computational result suggests that both cartilage with complete meniscectomy and that with full thickness defect are less able to support joint loading through interstitial fluid pressurization, even for a relatively short period of time (e.g. both cartilages reach 90% consolidation in about 15 min).

The simulation result shows a similar DoC for cartilage with partial meniscectomy (Case 2) and for that with a partial thickness defect (Case 4) although they have different peak contact strain at any given time (see Figure 4.a and 4.b). This result suggests that a

partial thickness defect (focal lesion) can have a similar negative impact on cartilage mechanical performance as a partial meniscectomy, although the final deformation with partial thickness defect is considerably smaller compared to that for cartilage with partial meniscectomy.

### 3.3. *Excess interstitial fluid pressure*

To help understand the predicted strain and DoC shown in Figure 4, in Figure 5 we plot the spatial distribution of the tissue excess interstitial fluid pressure for each case at two time-points: at the start of load (a:  $t=5$  s) and near steady state (b:  $t=1$  hr). Figure 5 illustrates that peak contact pressure (maximum pressure underneath the load) is relatively higher for cartilage with meniscectomy (Case 2 and 3) at the early stage of loading due to their higher load per unit area. Although the cartilage model with full thickness defect (Case 5) experiences a larger load per unit area compared to the meniscectomy models, it has a smaller fluid pressure at  $t=5$  s due to its increased free drainage surface area in the defect region (see results in next section on fluid exudation).

As illustrated in Figure 5b the intact cartilage experiences the largest excess interstitial fluid pressure among all cases after the load has been continuously applied for  $t=1$  hr. This result indicates that for the intact cartilage, the interstitial fluid bears a relatively larger portion of the load, and a smaller part of the load is supported by cartilage solid matrix, leading to a smaller effective stress and so a lower risk of frictional wear. The small excess interstitial fluid pressure at  $t=1$  hr (due to large water exudation), as predicted for Cases 3 to 5, results in a large portion of the load being supported by the cartilage solid matrix.

### 3.4. Fluid exudation volume and rate

Consolidation of cartilage tissue is a result of interstitial fluid exudation following the loading application. To help better understand cartilage consolidation behaviour and its relationship with cartilage surface wear, we plot the computational predictions of exudate flow rate and total exudate volume for the five cases in Figure 6.a and 6.b. The largest exudate flow rate is predicted for the cartilage with full thickness defect (Case 5) at the early stage (i.e.  $t < 10$  min). However, the flow rate is predicted to decline sharply with time for this case and is negligible at approximately  $t = 45$  min, as the cartilage is then fully consolidated. An initial relatively high exudate flow rate is also predicted for complete meniscectomy (Case 3), due to its highest early excess interstitial fluid pressure as well as its relatively short drainage (i.e. high pressure gradient), compared to that of intact cartilage. As expected, the exudate flow rate for this case decreases relatively quickly with time (Figure 6.a), resulting in the lowest total exudate volume (Figure 6.b). As indicated in Figure 6.a, the intact cartilage (Case 1) can sustain its fluid exudation for a longer period of time compared to all other cases, suggesting the ability of intact cartilage to support joint movement through interstitial fluid pressurization for sustained period.

Figure 6.c illustrates the time evolution of normalized exudate volume, average DoC, average normal effective stress and average excess interstitial fluid pressure for healthy cartilage (Case 1). It can be seen that there is a strong correlation between DoC, exudate volume and effective stress, while the excess interstitial fluid pressure is complementary. A small DoC indicates a small fluid exudate volume and a small effective stress on the cartilage surface, while a large DoC ( $\text{DoC} \rightarrow 1$ ), which happens under sustained loading condition, indicates a large exudate volume and consequently a large load share carried by the solid

matrix (i.e. large effective stress). Sliding with a large effective normal stress may result in damage of cartilage extracellular matrix and frictional wear of the cartilage surface.

#### 4. Discussion

One of the main factors which can strongly influence cartilage biomechanical performance and its ability to support joint loading without interfacial wear and tissue degeneration is the friction coefficient between opposing cartilage surfaces. It has been suggested that application of sustained stationary loading on articular cartilage increases the subsequent apparent friction coefficient (Forster and Fisher, 1996; Forster and Fisher, 1999). Following the application of a physiologically-relevant stationary loading with duration ranging from 2 to 45 min, Forster and Fisher (1996) measured the apparent contact friction coefficient of cartilage in the presence of synovial fluid lubricant. The apparent friction coefficient increased progressively from a low of 0.025 after 2 min stationary loading application to a high of 0.25 after 45 min stationary loading. The authors found that the apparent friction coefficient was dependent on the duration of the stationary load applied on the cartilage. They speculated that the time-dependent load carried by the fluid phase is primarily responsible for low apparent friction coefficient of cartilage (Forster and Fisher, 1996; Forster and Fisher, 1999).

To test the hypothesis of our study (i.e. that the duration of cartilage loading relative to the characteristic time for cartilage consolidation plays an important role in determining the friction coefficient and so the rate of cartilage damage and wear), we plot both apparent friction coefficient obtained from Forster and Fisher (1996)'s experimental result and the DoC (for intact cartilage) from our computational result (Figure 7.a). The results show that both DoC and apparent friction coefficient increase with respect to loading time with a

similar rate, confirming the hypothesis defined in our study is valid. This is consistent with the view that the apparent friction coefficient in articular cartilage increases as the load is progressively transferred from the interstitial fluid to the extra cellular matrix. The result is also consistent with the experimental measurements of Krishnan et al. (2004) that show a very strong and linear negative correlation between friction coefficient and interstitial fluid pressure ( $r^2=0.96\pm 0.03$ ) for bovine articular cartilage disks while sliding against glass under a constant loading. As indicated in Figure 6.c, upon initial loading, a large part of the normal load is supported by pressurized interstitial fluid (i.e. by the large excess fluid pressure), while a small load is carried by solid matrix (i.e. small effective stress). In fact a large fraction of the total stress at the interface is supported by fluid at the early stage of loading (Pierce et al., 2016), leading to a low apparent friction coefficient due to negligible friction force between fluid particles. This mode of lubrication, also known as hydrostatic lubrication (or hydrodynamic lubrication in case of dynamic loading), is the dominant lubrication regime at the onset of static (or dynamic) loading (Krishnan et al., 2004; Neu et al., 2008; Pierce et al., 2016). With increasing duration of loading, the contribution of the load carried by the fluid phase decreases, with load increasingly transferred to the solid phase. This rising solid phase load leads to increasing number and size of asperity contacts and a commensurate rise in friction force (Ateghian, 2009; Forster and Fisher, 1996; Forster and Fisher, 1999; McCutchen, 1959). The lubrication regime, known as mixed mode lubrication, is a transition from hydrostatic (or hydrodynamic) lubrication mode (resulting from load support by the fluid phase) at the early stage of loading to boundary lubrication mode (resulting from load support by the solid phase and asperity contacts) at the late stage (Caligaris and Ateghian, 2008; Neu et al., 2008). Asperity contact of opposing cartilage surfaces leads to cartilage surface damage and wear (McNary et al., 2012; Scherge et al., 2001).

Following the aforementioned description, the surface shear stress  $\tau$  (i.e. friction force per unit area) between the cartilage contacting surfaces can be written as:

$$\tau = \mu_{app} \times \sigma \quad (9)$$

where  $\mu_{app}$  is apparent friction coefficient and  $\sigma$  is the normal total stress at the surface (see Equation 1). For biphasic cartilage, surface shear stress can be decomposed into fluid and solid components. Since the frictional force between fluid particles is ignorable, the surface shear stress can be expressed as follows:

$$\tau = \mu_T \times \sigma_E^S \quad (10)$$

Where  $\mu_T$  is true friction coefficient (i.e. cartilage solid matrix on cartilage solid matrix friction coefficient) and  $\sigma_E^S$  is normal effective stress at the surface (i.e. the normal stress at the surface carried by cartilage solid matrix). Therefore:

$$\mu_{app} = \mu_T \times \frac{\sigma_E^S}{\sigma} \quad (11)$$

As indicted in Figure 6.c, DoC can be used to estimate  $\sigma_E^S/\sigma$ . So the apparent friction coefficient can be estimated using DoC (note that  $\mu_T$  is constant):

$$\mu_{app} = \mu_T \times DoC \quad (12)$$

Figure 7.a and b confirm the above relationship between DoC and the apparent friction coefficient, In Figure 7.b we plot the apparent friction coefficient measured by Forster and Fisher (1996) against our simulation results of cartilage DoC. It can be seen that there is a very strong positive linear correlation between apparent friction coefficient and DoC indicating that the hypothesis defined in this paper is valid. This result suggests that the DoC can be used as an index to describe the cartilage lubrication condition and risk of frictional wear. In other words, the results of this study suggest that, we can infer the friction coefficient between opposing cartilage surfaces from the degree of joint space narrowing

over time (i.e. DoC vs time) obtained using medical imaging of the joint. This can potentially have a significant application in experimental studies and clinical practice since it allows a non-invasive evaluation of the articular cartilages friction coefficient and subsequently joint health. Hosseini et al. (2010) have previously used a combined Dual Fluoroscopic Imaging System (DFIS) and MRI technique to measure the in-vivo tibio-femoral cartilage deformation over time for the study participants who applied full body weight on single leg for 300 s. This technique or similar techniques can be potentially used in clinical practice to measure the rate of consolidation of tibio-femoral cartilage when the patient applies full body weight on their knees to estimate their knee joints friction coefficient and evaluate knees articulation health. This proposed medical examination can be conducted by a combined Dual Fluoroscopic Imaging and MRI imaging of the knee for at least 3 times (e.g. 1 min, 5 min and 15 min after the load application) while the patient applies a full body weight on their knees (e.g. for 15 min). Following the examination, the tibio-femoral cartilage deformation over time can be measured from the images and the DoC vs time can be plotted (see Figure 7.a). By comparing the patient's examination result of the rate of consolidation (i.e. DoC vs time) against the developed database, his/her knee articulation health can potentially be assessed. It should be mentioned that, the patient should be asked to avoid any strenuous activity such as running, lifting and stairclimbing at least 4 hrs prior to the examination. In addition, the patient should be asked to refrain from weight bearing for 1 hr prior the imaging to ensure the knees cartilages are totally recovered from any residual deformation (Bingham et al., 2008).

It is worth mentioning that, by extrapolating Figure 7.a, the apparent friction coefficient when cartilage is fully consolidated (i.e. the true friction coefficient for cartilage

on cartilage in the presence of synovial fluid) is predicted to be 0.35. Forster and Fisher (1996) showed that after application of stationary loading for 45 min, then unloading cartilage specimens for 1 min, followed by a re-application of stationary load for another 5 s, the apparent friction coefficient temporarily decreases sharply from 0.25 to 0.04. This highlights the importance of re-imbibition of interstitial fluid upon unloading in maintaining a low friction coefficient in the joints. In other words, the lubrication mechanism in knee joints suits reciprocating loads (i.e. walking and running), while application of sustained static loading on articular cartilage can result in significantly higher friction coefficient (as measured by Forster and Fisher (1996)) and consequently larger risk of frictional wear of the cartilage surface.

It should be noted that this study has some limitations. To simplify the problem, we assumed an axisymmetric geometry and loading condition for lateral tibial plateau. Further it was assumed that bodyweight loading is equally distributed between the lateral and medial compartments of tibial cartilage with the same contact areas. A future study could apply the model developed in this paper to a 3D geometry of the total knee joint reconstructed based on CT scan images to further investigate the influence of knee geometry and loading conditions on tibio-femoral cartilage mechanical environment.

It is also worth mentioning that, in the model developed in this study, a zero-flux (i.e. impermeable) boundary condition was assumed in the contact region. This was following the same boundary condition included in Ateshian et al's study (1994) that suggested that the contact problem of two opposing biphasic articular cartilages with similar geometry and materials properties is equivalent to a rigid impermeable plane contacting one of the two articular cartilages. However in reality there could be some limited outward flux from the

cartilage (known as weeping lubrication (Lewis and McCutchen, 1959)) as well as some inward flux to the cartilage (known as boosted lubrication (Walker et al., 1968)) in the contact region. In other words, some studies suggesting that there is interstitial fluid exudation between two contacting articular cartilages, a process known as weeping lubrication (Lewis and McCutchen, 1959), whereas some other investigations suggest when two opposing articular cartilages are pressed against each other, water molecules of synovial fluid penetrate to the tissue and leave a concentrated synovial fluid between the cartilages, a process called boosted lubrication (Walker et al., 1968). It is still a matter of debate whether there is no fluid flow between two contacting cartilages and joint space or there is an inward or outward flux or combination of these mechanisms (Ateshian, 2004, 2009). In this study we assumed there is no flux in the contact region, which is an intermediate position between having an inward or outward flux.

## 5. Conclusion

The present work simulated the mechanical response of articular cartilage to sustained period of static loading and compared the response of intact cartilage with those of injured cartilage and joints. The main conclusions of this paper can be summarized as follows.

The main conclusions of this paper can be summarized as follows.

- The intact cartilage, in contrast to complete and partial meniscectomy and the presence of defects, is predicted to have the most sustained interstitial fluid

pressurisation and (related) time to reach maximum consolidation, both of which are expected to be favourable to minimizing cartilage damage and wear.

- The cartilage with complete meniscectomy is predicted to experience the largest strains, and so be most exposed to tissue extracellular matrix damage and chondrocyte apoptosis. In addition, both cartilage with complete meniscectomy and that with full thickness defect display the most rapid consolidation and would then be expected to be more exposed to increased wear at the cartilage surface associated with more frequent bouts of higher friction coefficients.
- A similar and relatively large consolidation rate is predicted for cartilage with partial meniscectomy and that with partial thickness defect although they experience different contact strain. This suggests that a focal lesion on cartilage surface can have similar negative impact on cartilage durability as partial meniscectomy although contact strain for cartilage with focal lesion is considerably smaller.
- There is a strong positive linear correlation between DoC of articular cartilage and apparent friction coefficient at the joints. This result suggests that we can evaluate the friction coefficient between opposing cartilage surfaces by medical imaging of the degree of joint space closure over time and consequently evaluate the joint articulation health in clinical practice.

### **Acknowledgements**

The authors would like to acknowledge the funding support of this project by the Australian Federal Government NH&MRC APP1051538 grant.

### **Conflict of interest**

There is no conflict of interest to declare.

Table 1 Material parameters applied in the computational model in this study

| Parameter             | Value                   | Reference                  |
|-----------------------|-------------------------|----------------------------|
| $\phi^f$              | 0.8                     | (Bonassar et al., 2000)    |
| $\phi_{G0}(z = 0)$    | 60 mg/ml                | (Wedig et al., 2005)       |
| $\phi_{G0}(z = -5mm)$ | 100 mg/ml               | (Wedig et al., 2005)       |
| $a_1$                 | 0.01 MPa                | (Treppo et al., 2000)      |
| $a_2$                 | 0.075 MPa               | (Treppo et al., 2000)      |
| $m$                   | -2.37                   | (Zamparo and Comper, 1989) |
| $n$                   | 5.4 e-22 m <sup>2</sup> | (Zamparo and Comper, 1989) |
| $\mu$ (at 37°C)       | 7 e-4 Ns/m <sup>2</sup> | (Kestin et al., 1978)      |

Table 2. Depth and orientation dependent cartilage material properties applied in this paper (Fox et al., 2009; Kempson et al., 1973)

| Location         | Tensile modulus (MPa) |          | Collagen volume fraction ( $\alpha$ ) | Shear modulus (MPa) |
|------------------|-----------------------|----------|---------------------------------------|---------------------|
|                  | Horizontal            | Vertical |                                       |                     |
| Superficial zone | 100                   | 25       | 45%                                   | 3                   |
| Middle zone      | 30                    | 10       | 30%                                   | 3                   |
| Deep zone        | 10                    | 15       | 25%                                   | 2                   |

Table 3 Experimental measurements of tibio-femoral contact area

| Contact area (mm <sup>2</sup> ) |              |                    |              | Loading applied on joint | Reference                        |
|---------------------------------|--------------|--------------------|--------------|--------------------------|----------------------------------|
| Lateral compartment             |              | Medial compartment |              |                          |                                  |
| Intact                          | Meniscectomy | Intact             | Meniscectomy |                          |                                  |
| 990                             | 590          | 1100               | 670          | 2200 N                   | (Macquet Paul et al., 1975)      |
| 983±281                         | 755±190      | 903±358            | 869±175      | 500 N                    | (Bai et al., 2001)               |
| 571±80                          | N/A          | 594±59             | N/A          | 1800 N                   | Marzo and Gurske-DePerio (2009)  |
| 510±70                          | 230±80       | 640±18             | 300±80       | 1000 N                   | (Fukubayashi and Kurosawa, 1980) |
| 200±50                          | N/A          | 320±90             | N/A          | Full bodyweight          | (Van de Velde et al., 2009)      |

Table 4 The lateral tibio-femoral contact area and loading applied in the cartilage models developed in this paper. It was assumed that 2.59 standard bodyweight (i.e. 2.59×750 N) was applied on the knee.

| Parameter                           | Case 1<br>(Intact cartilage) | Case 2<br>(Cartilage with partial meniscectomy) | Case 3<br>(Cartilage with complete meniscectomy) | Case 4<br>(Cartilage with partial thickness defect) | Case 5<br>(Cartilage with full thickness defect) |
|-------------------------------------|------------------------------|---|--|---|--|
| Contact area (mm <sup>2</sup> )     | 500                          | 365   | 235  | 490   | 370  |
| Resultant applied force (N)         | 970                          | 970   | 970  | 970   | 970  |
| Peak loading per unit area (MPa)    | 5.8                          | 8   | 12.7   | 6.2   | 12.2   |
| Average loading per unit area (MPa) | 1.94                         | 2.66  | 4.13   | 1.97  | 2.62   |

Table 5 Consolidation rates for the five different cartilage cases simulated in this study

| Degree of consolidation | Consolidation time (minutes) |   |  |   |  |
|-------------------------|------------------------------|---|--|---|--|
|                         | Case 1<br>(Intact cartilage) | Case 2<br>(Cartilage with partial meniscectomy) | Case 3<br>(Cartilage with complete meniscectomy) | Case 4<br>(Cartilage with partial thickness defect) | Case 5<br>(Cartilage with full thickness defect) |
| 50%                     | 16                           | 9   | 3  | 5.5   | 0.6  |
| 80%                     | 52                           | 30  | 10   | 26  | 5.5  |
| 90%                     | 82                           | 50  | 15   | 44  | 12   |
| 99%                     | 179                          | 125   | 30   | 106   | 38   |

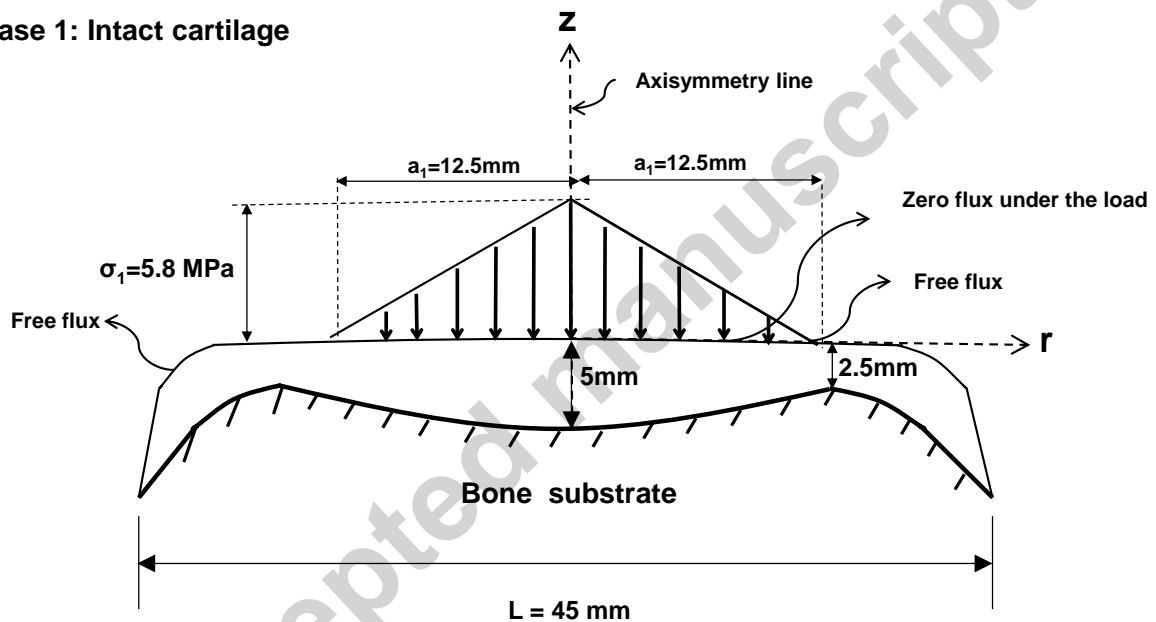
**Case 1: Intact cartilage**

Figure 1 Axisymmetric model geometry and boundary conditions for the intact lateral tibial plateau cartilage (case 1). It was assumed that a static conically-distributed load with a resultant force of 970 N ( $F_R=970$  N) was applied on lateral tibial plateau cartilage with a contact area of  $500 \text{ mm}^2$  ( $r=a_1=12.5$  mm) (Fukubayashi and Kurosawa, 1980). The loading distribution and contact area represent tibio-femoral contact loading condition under one legged stance loading (Kutzner et al., 2010) and under presence of menisci. A zero fluid flux boundary condition was assumed under the load while the unloaded surface of the cartilage was considered to have free flux condition. Note that the model is axisymmetric around z axis.

Case 2: **Cartilage with partial meniscectomy**

Case 3: **Cartilage with complete meniscectomy**

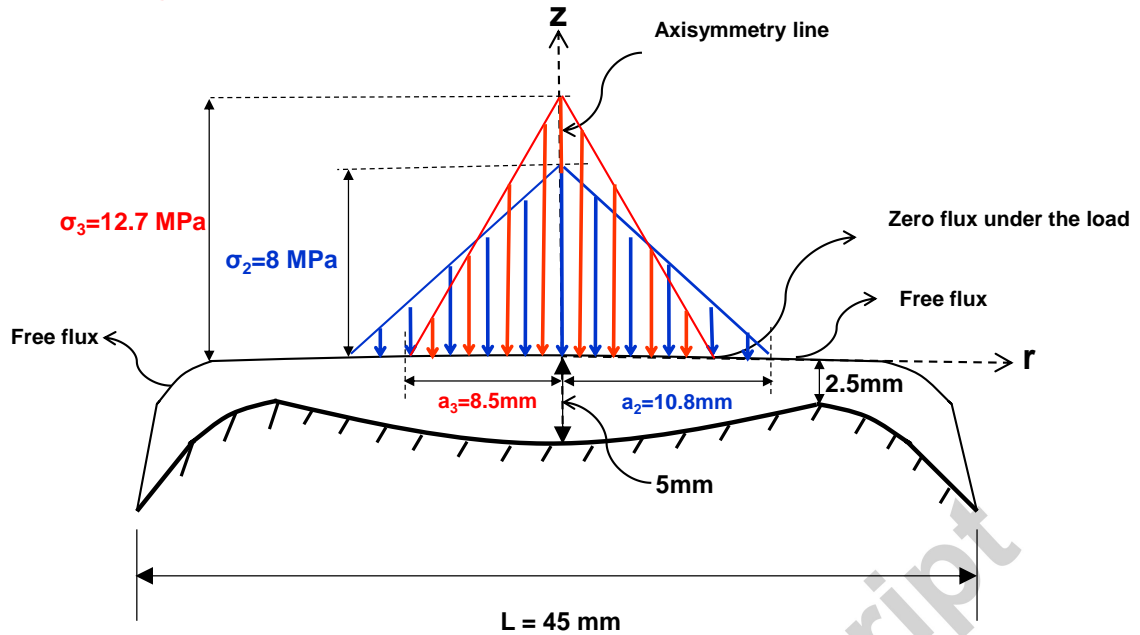
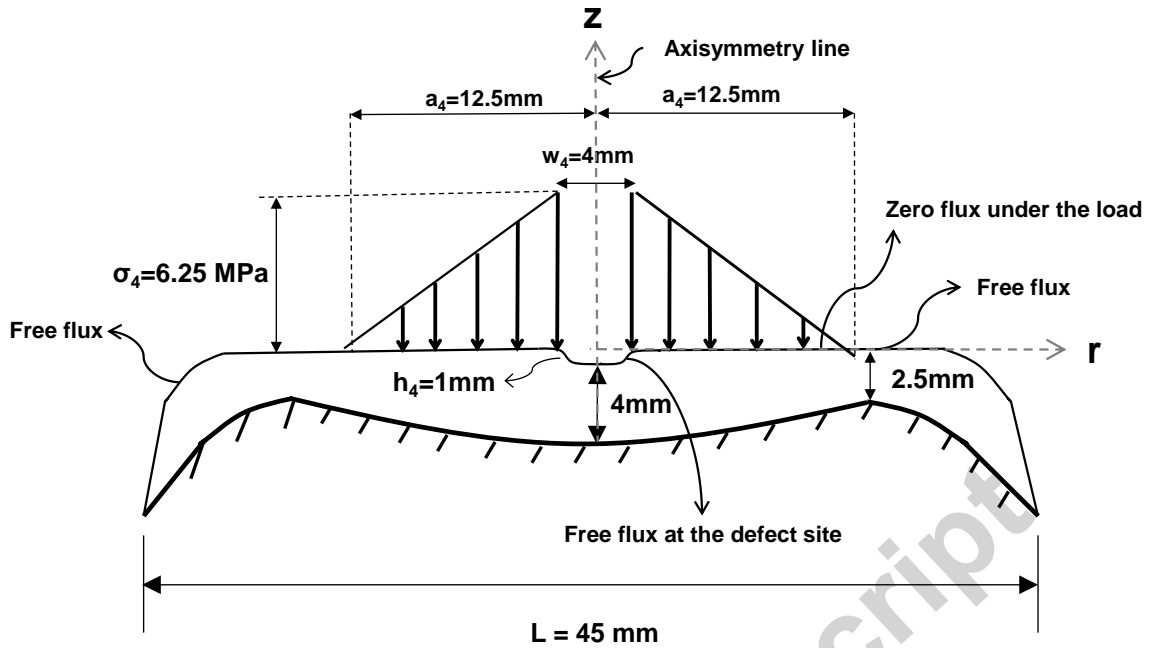


Figure 2 Axisymmetric model geometry and boundary conditions for lateral tibial plateau cartilage with partial meniscectomy (case 2) and complete meniscectomy (case 3). Note that the same resultant contact load (as the intact cartilage model) was applied on the meniscectomy models ( $F_R=970$  N), but over a small contact areas. The lateral plateau contact area without menisci (complete meniscectomy) was assumed to be  $235 \text{ mm}^2$  ( $r=a_3=8.5$  mm) (Fukubayashi and Kurosawa, 1980). For partial meniscectomy, an intermediate contact area of  $365 \text{ mm}^2$  was considered ( $r=a_2=10.8$  mm). The reduced contact area for meniscectomy model results in a larger peak loading and subsequently a larger contact pressure.

## (a) Case 4: Cartilage with partial thickness defect



## (b) Case 5: Cartilage with full thickness defect

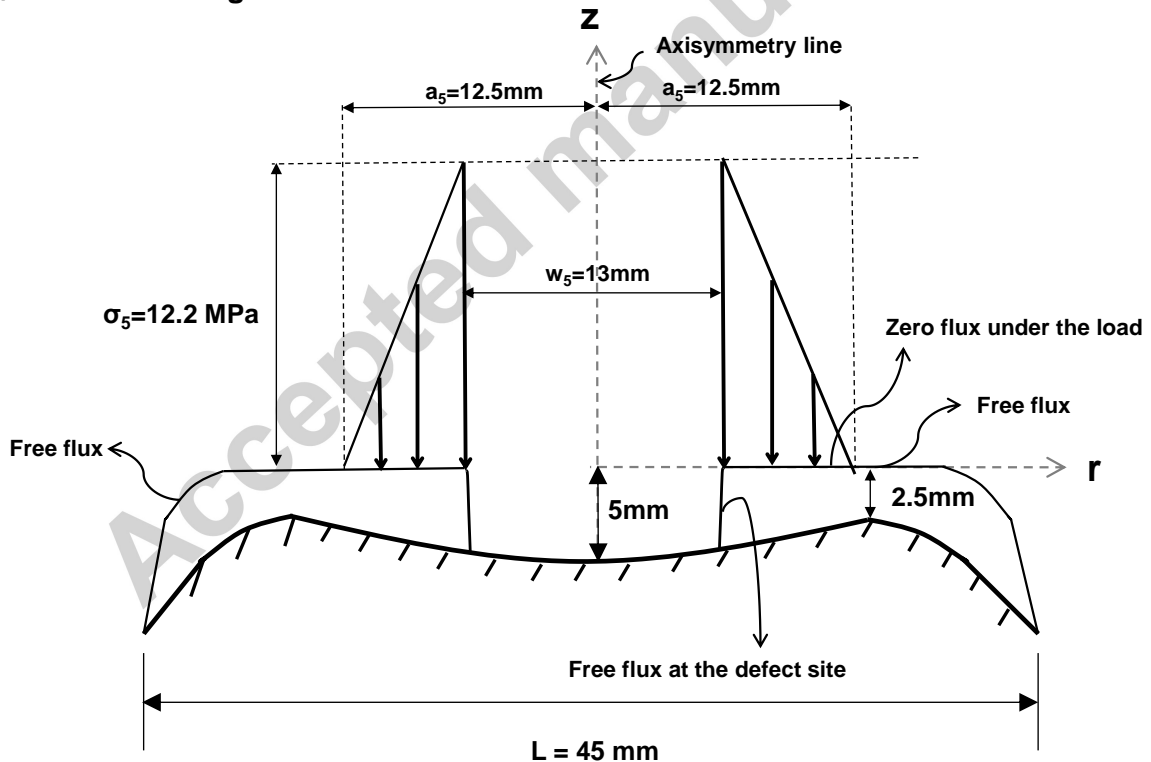
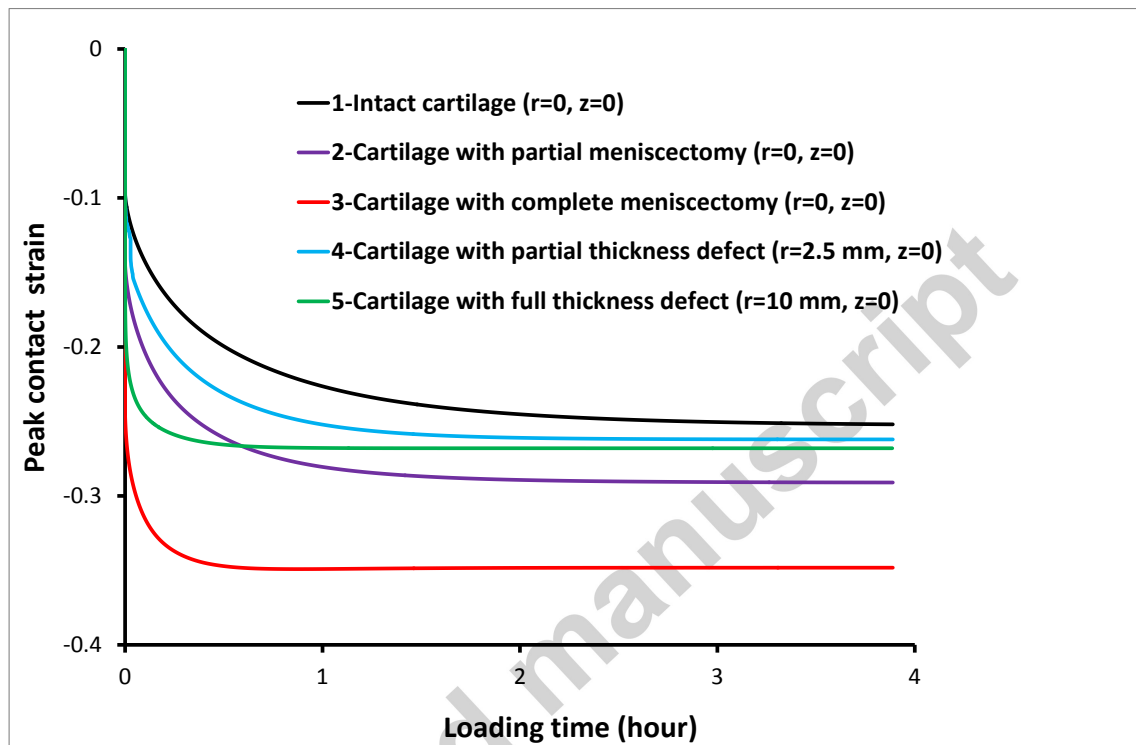


Figure 3 Model geometry and boundary conditions for lateral tibial plateau cartilage with partial thickness defect (case 4) and that with full thickness defect (case 5). Note that the same resultant contact load (as the intact cartilage model) was applied on the cartilage with defect models ( $F_R = 970$

N), however, the load was applied over a smaller surface area, as a result of surface damage for cartilage with defect. This leads to a larger load per unit area for cartilages with defect compared to the intact cartilage model. In addition there was a free flux boundary condition at the defect site as a result of removal of tissue and non-contact condition. This situation can accelerate the cartilage tissue exudation under loading.

(a)



(b)

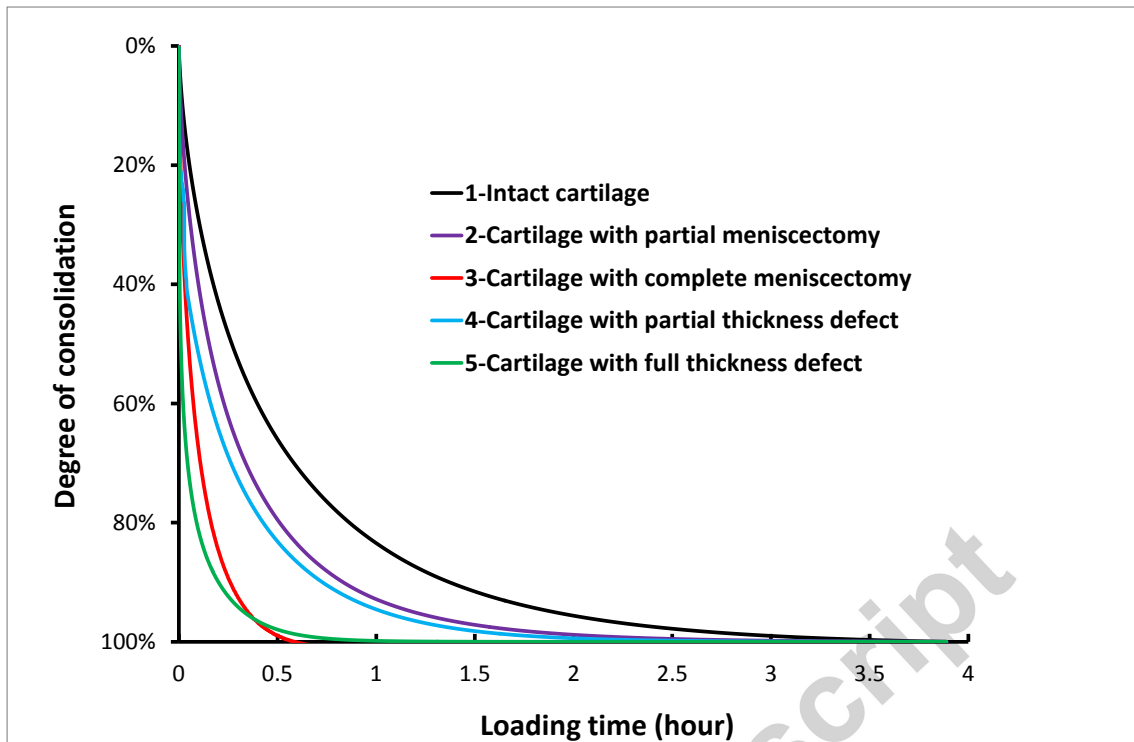


Figure 4 (a) Time evolution of peak contact strain for five cartilage models investigated in this study. The coordinate in brackets shows the location of the peak contact strain. It can be seen that the cartilage models with meniscectomy experience largest contact strain while the cartilage model with full thickness defect experiences the highest rate of strain rise. Figure 4 (b) illustrates degree of consolidation versus time for different cartilage models.

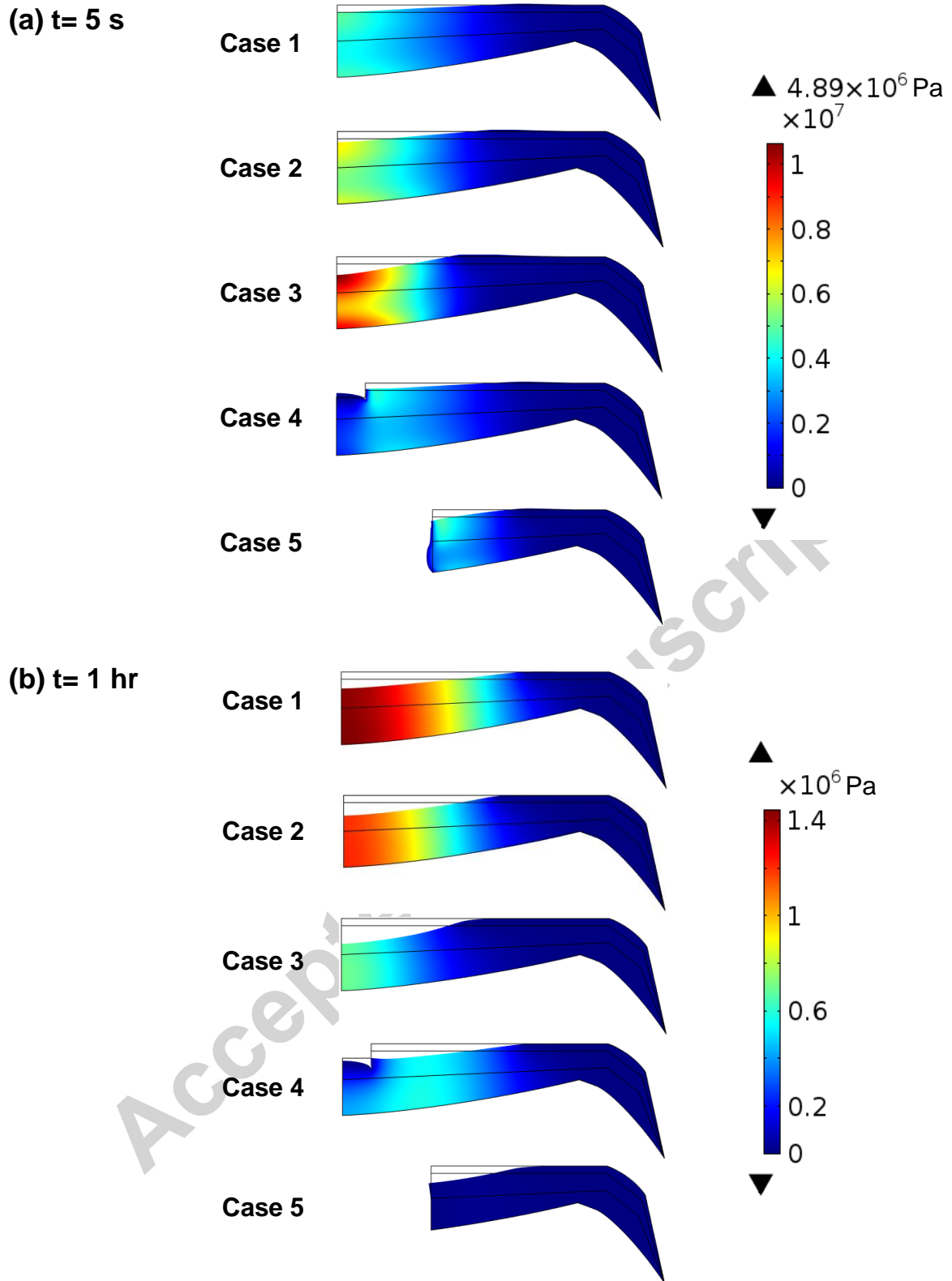
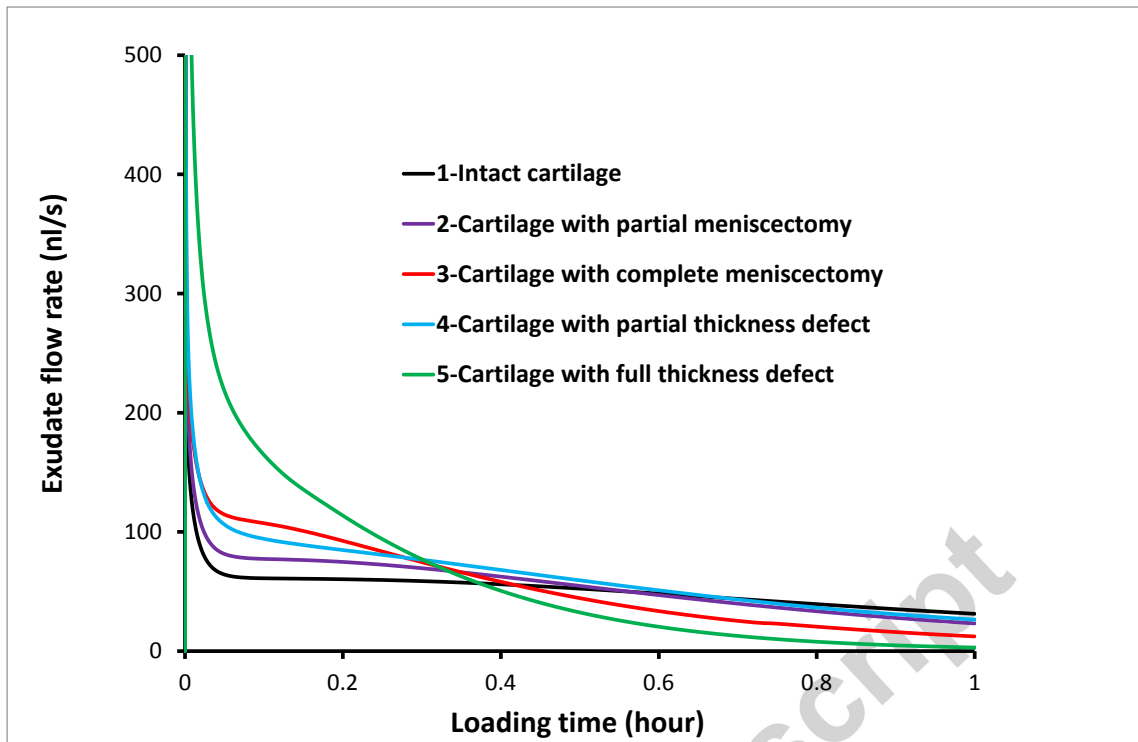
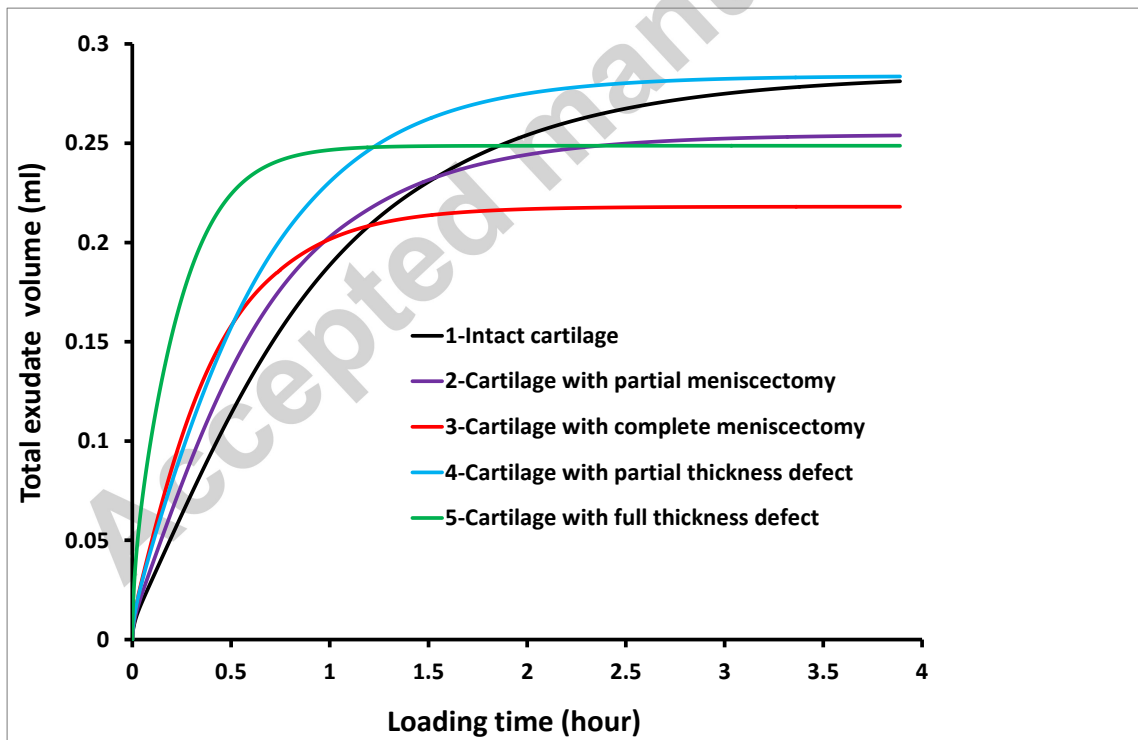


Figure 5 Distribution of excess interstitial fluid pressure after application of stationary loading for (a)  $t=5 \text{ s}$  and (b)  $t=1 \text{ hr}$ . Please note the different pressure colour scales between (a) and (b). Deformation scale=1 for both (a) and (b).

(a)



(b)



(c)

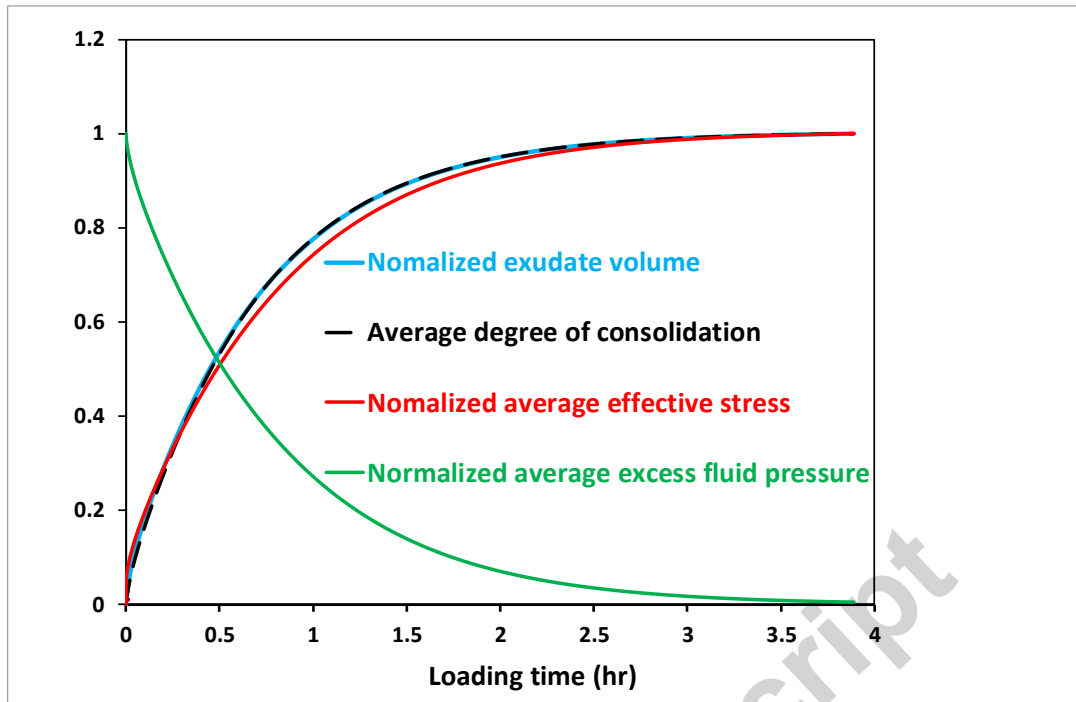
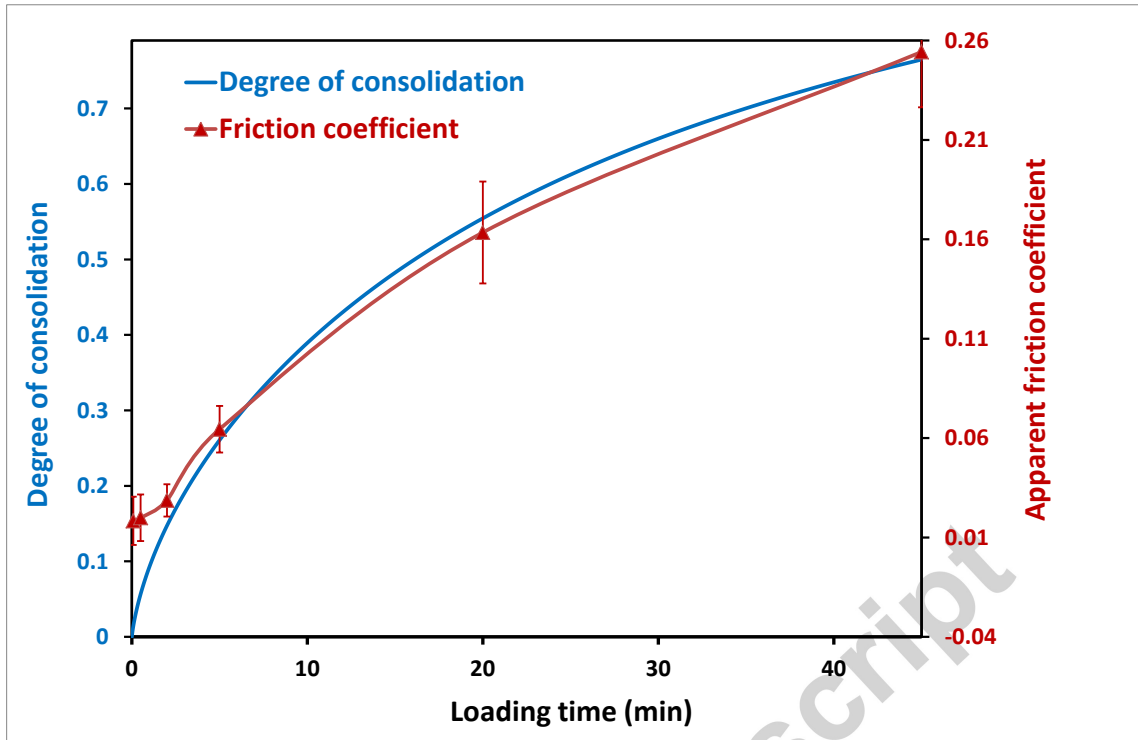


Figure 6 (a) The exudate flow rate versus time for cartilage models investigated in this paper. The model predicts a larger exudate flow rate for the model with full thickness defect at the early stage of loading in comparison with other models. It can be seen that the exudate flow rate for the cartilage with full thickness defect and that with complete meniscectomy (Case 5 and 3) is predicted to drop to zero relatively quickly in comparison with other models. Figure 6 (b) Volume of total exudate versus time for different cases. It can be seen that the total exudate volume is smallest for intact cartilage at the early stage of loading while it continues to increase even after three hours of loading. Figure 6 (c) The time evolution of normalized exudate volume, average degree of consolidation, normalized average effective stress and normalized average excess fluid pressure for healthy cartilage (Case 1)

(a)



(b)

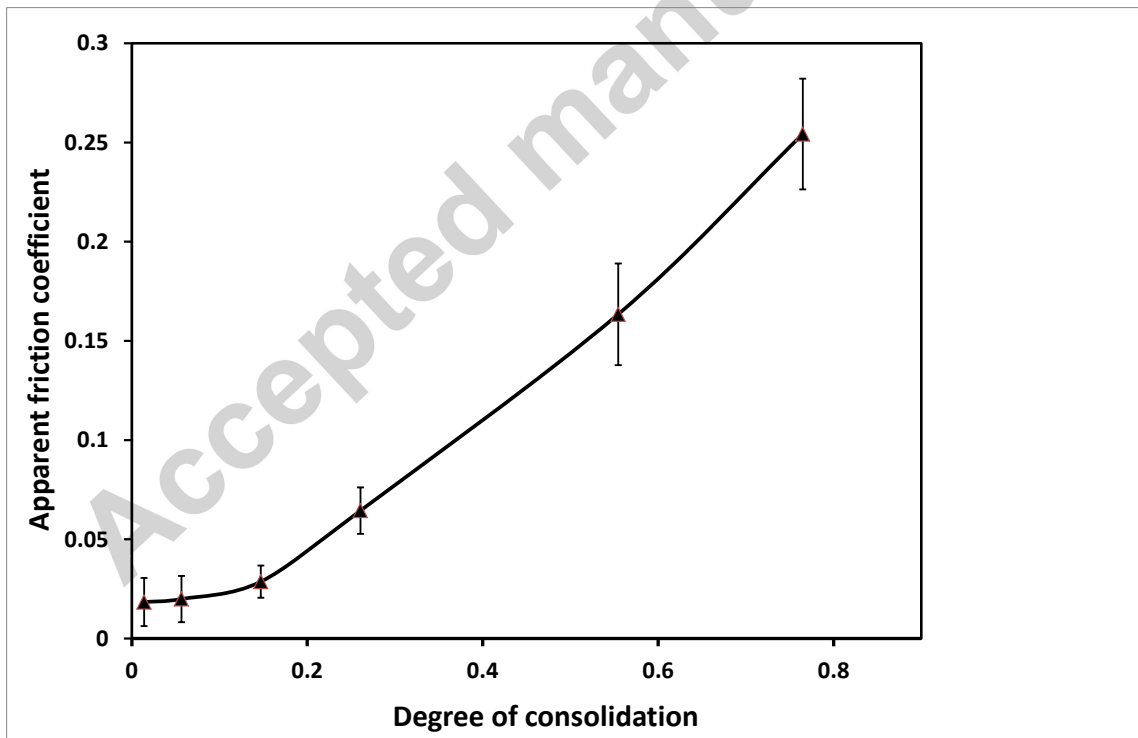


Figure 7 (a) Time evolution of intact cartilage consolidation (obtained from computational simulation result in this study) and apparent friction coefficient of cartilage on cartilage contact obtained from experimental result of Forster and Fisher (1996). As can be seen from Figure 7 (b), there is a strong

positive linear correlation between cartilage apparent friction coefficient and its degree of consolidation.

## References

- Ateshian, G., Lai, W., Zhu, W., Mow, V., 1994. An asymptotic solution for the contact of two biphasic cartilage layers. *J. Biomech.* 27, 1347-1360.
- Ateshian, G.A., 2004. Response to Comment by Charles W. McCutchen. *Transactions of the ASME-K-Journal of Biomechanical Engineering* 126, 537-537.
- Ateshian, G.A., 2009. The role of interstitial fluid pressurization in articular cartilage lubrication. *J. Biomech.* 42, 1163-1176.
- Bai, B., Kummer, F.J., Sala, D.A., Koval, K.J., Wolinsky, P.R., 2001. Effect of articular step-off and meniscectomy on joint alignment and contact pressures for fractures of the lateral tibial plateau. *J. Orthop. Trauma* 15, 101-106.
- Barker, M., Seedhom, B., 2001. The relationship of the compressive modulus of articular cartilage with its deformation response to cyclic loading: does cartilage optimize its modulus so as to minimize the strains arising in it due to the prevalent loading regime? *Rheumatology* 40, 274-284.
- Bingham, J., Papannagari, R., Van de Velde, S., Gross, C., Gill, T., Felson, D., Rubash, H., Li, G., 2008. In vivo cartilage contact deformation in the healthy human tibiofemoral joint. *Rheumatology* 47, 1622-1627.
- Bonassar, L.J., Grodzinsky, A.J., Srinivasan, A., Davila, S.G., Trippel, S.B., 2000. Mechanical and physiochemical regulation of the action of insulin-like growth factor-i on articular cartilage. *Archives of Biochemistry and Biophysics* 379, 57-63.
- Caligaris, M., Ateshian, G.A., 2008. Effects of sustained interstitial fluid pressurization under migrating contact area, and boundary lubrication by synovial fluid, on cartilage friction. *Osteoarthritis Cartilage* 16, 1220-1227.
- Forster, H., Fisher, J., 1996. The influence of loading time and lubricant on the friction of articular cartilage. *Proceedings of the Institution of Mechanical Engineers* 210, 109-119.

- Forster, H., Fisher, J., 1999. The influence of continuous sliding and subsequent surface wear on the friction of articular cartilage. *Proceedings of the Institution of Mechanical Engineers, Part H: Journal of Engineering in Medicine* 213, 329-345.
- Fox, A.J.S., Bedi, A., Rodeo, S.A., 2009. The basic science of articular cartilage: structure, composition, and function. *Sports Health: A Multidisciplinary Approach* 1, 461-468.
- Fukubayashi, T., Kurosawa, H., 1980. The contact area and pressure distribution pattern of the knee: a study of normal and osteoarthrotic knee joints. *Acta Orthop. Scand.* 51, 871-879.
- Gardiner, B., Smith, D., Pivonka, P., Grodzinsky, A., Frank, E., Zhang, L., 2007. Solute transport in cartilage undergoing cyclic deformation. *Computer methods in biomechanics and biomedical engineering* 10, 265-278.
- Gardiner, B.S., Woodhouse, F.G., Besier, T.F., Grodzinsky, A.J., Lloyd, D.G., Zhang, L., Smith, D.W., 2016. Predicting knee osteoarthritis. *Ann. Biomed. Eng.* 44, 222-233.
- Goodwin, D., Wadghiri, Y., Zhu, H., Vinton, C., Smith, E., Dunn, J., 2004. Macroscopic Structure of Articular Cartilage of the Tibial Plateau: Influence of a Characteristic Matrix Architecture on MRI Appearance. *AJR, American journal of roentgenology* 182, 311-318.
- Hayes, W., Swenson, L., Schurman, D., 1978. Axisymmetric finite element analysis of the lateral tibial plateau. *J. Biomech.* 11, 21-33.
- Hosseini, A., Van de Velde, S.K., Kozanek, M., Gill, T.J., Grodzinsky, A.J., Rubash, H.E., Li, G., 2010. In-vivo time-dependent articular cartilage contact behavior of the tibiofemoral joint. *Osteoarthritis Cartilage* 18, 909-916.
- Kempson, G., Muir, H., Pollard, C., Tuke, M., 1973. The tensile properties of the cartilage of human femoral condyles related to the content of collagen and glycosaminoglycans. *Biochimica et Biophysica Acta (BBA)-General Subjects* 297, 456-472.
- Kestin, J., Sokolov, M., Wakeham, W.A., 1978. Viscosity of liquid water in the range  $-8^{\circ}\text{C}$  to  $150^{\circ}\text{C}$ . *Journal of Physical and Chemical Reference Data* 7, 941-948.
- Krishnan, R., Kopacz, M., Ateshian, G.A., 2004. Experimental verification of the role of interstitial fluid pressurization in cartilage lubrication. *J. Orthop. Res.* 22, 565-570.

- Kutzner, I., Heinlein, B., Graichen, F., Bender, A., Rohlmann, A., Halder, A., Beier, A., Bergmann, G., 2010. Loading of the knee joint during activities of daily living measured in vivo in five subjects. *J. Biomech.* 43, 2164-2173.
- Kwan, M.K., Lai, W.M., Van Mow, C., 1984. Fundamentals of fluid transport through cartilage in compression. *Ann. Biomed. Eng.* 12, 537-558.
- Lewis, P., McCutchen, C., 1959. Mechanism of animal joints: experimental evidence for weeping lubrication in mammalian joints. *Nature* 184, 1285.
- Longmore, R.B., Gardner, D.L., 1975. Development with age of human articular cartilage surface structure. A survey by interference microscopy of the lateral femoral condyle. *Ann. Rheum. Dis.* 34, 26-37.
- Macquet Paul, G., Van de Berg André, J., Simonet Jacques, C., 1975. Femorotibial Weight-Bearing Areas. *The Journal of Bone and Joint Surgery*, 766-771.
- Marzo, J.M., Gurske-DePerio, J., 2009. Effects of medial meniscus posterior horn avulsion and repair on tibiofemoral contact area and peak contact pressure with clinical implications. *The American journal of sports medicine* 37, 124-129.
- McCutchen, C., 1959. Sponge-hydrostatic and weeping bearings. *Nature* 184, 1284.
- McDermott, I., Amis, A., 2006. The consequences of meniscectomy. *Journal of Bone & Joint Surgery, British Volume* 88, 1549-1556.
- McNary, S.M., Athanasiou, K.A., Reddi, A.H., 2012. Engineering lubrication in articular cartilage. *Tissue Engineering Part B: Reviews* 18, 88-100.
- Merkher, Y., Sivan, S., Etsion, I., Maroudas, A., Halperin, G., Yosef, A., 2006. A rational human joint friction test using a human cartilage-on-cartilage arrangement. *Tribology Letters* 22, 29-36.
- Mow, V.C., Huiskes, R., 2005. *Basic orthopaedic biomechanics & mechano-biology*. Lippincott Williams & Wilkins.
- Mow, V.C., Ratcliffe, A., Poole, A.R., 1992. Cartilage and diarthrodial joints as paradigms for hierarchical materials and structures. *Biomaterials* 13, 67-97.
- Neu, C.P., Komvopoulos, K., Reddi, A.H., 2008. The interface of functional biotribology and regenerative medicine in synovial joints. *Tissue Engineering Part B: Reviews* 14, 235-247.

- Pierce, D., Ricken, T., Holzapfel, G.A., 2013. Modeling sample/patient-specific structural and diffusional responses of cartilage using DT-MRI. *International journal for numerical methods in biomedical engineering* 29, 807-821.
- Pierce, D.M., Unterberger, M.J., Trobin, W., Ricken, T., Holzapfel, G.A., 2016. A microstructurally based continuum model of cartilage viscoelasticity and permeability incorporating measured statistical fiber orientations. *Biomechanics and modeling in mechanobiology* 15, 229-244.
- Scherge, M., Gorb, S., Gorb, S.N., 2001. *Biological micro-and nanotribology*. Springer Science & Business Media.
- Soltz, M.A., Ateshian, G.A., 2000. A conewise linear elasticity mixture model for the analysis of tension-compression nonlinearity in articular cartilage. *J. Biomech. Eng.* 122, 576-586.
- Song, Y., Greve, J., Carter, D., Giori, N., 2008. Meniscectomy alters the dynamic deformational behavior and cumulative strain of tibial articular cartilage in knee joints subjected to cyclic loads. *Osteoarthritis Cartilage* 16, 1545-1554.
- Taylor, W.R., Heller, M.O., Bergmann, G., Duda, G.N., 2004. Tibio-femoral loading during human gait and stair climbing. *J. Orthop. Res.* 22, 625-632.
- Treppo, S., Koepp, H., Quan, E.C., Cole, A.A., Kuettner, K.E., Grodzinsky, A.J., 2000. Comparison of biomechanical and biochemical properties of cartilage from human knee and ankle pairs. *J. Orthop. Res.* 18, 739-748.
- Van de Velde, S.K., Bingham, J.T., Hosseini, A., Kozanek, M., DeFrate, L.E., Gill, T.J., Li, G., 2009. Increased tibiofemoral cartilage contact deformation in patients with anterior cruciate ligament deficiency. *Arthritis Rheum.* 60, 3693-3702.
- Verruijt, A., 2013. *Theory and problems of poroelasticity*. Delft University of Technology.
- Walker, P., Dowson, D., Longfield, M., Wright, V., 1968. " Boosted lubrication" in synovial joints by fluid entrapment and enrichment. *Ann. Rheum. Dis.* 27, 512.
- Wedig, M., Bae, W., Temple, M., Sah, R., Gray, M., 2005. GAG profiles in normal human articular cartilage, *Procs Orthopedic Research Society Meeting*, Washington DC.
- Zamparo, O., Comper, W.D., 1989. Hydraulic conductivity of chondroitin sulfate proteoglycan solutions. *Arch. Biochem. Biophys.* 274, 259-269.

Zhang, L., Gardiner, B.S., Smith, D.W., Pivonka, P., Grodzinsky, A., 2007. The effect of cyclic deformation and solute binding on solute transport in cartilage. *Arch. Biochem. Biophys.* 457, 47-56.

Zhang, L., Miramini, S., Gardiner, B.S., Smith, D.W., Grodzinsky, A.J., 2015. Time evolution of deformation in a human cartilage under cyclic loading. *Ann. Biomed. Eng.* 43, 1166-1177.

Accepted manuscript